University of Glasgow
DEPARTMENT OF
AEROSPACE
ENGINEERING

Multidomain Solutions of Incompressible Flows with Complex Geometry by Generalized Differential Quadrature

Chang SHU and Bryan E. RICHARDS

G.U. Aero. Report 9118

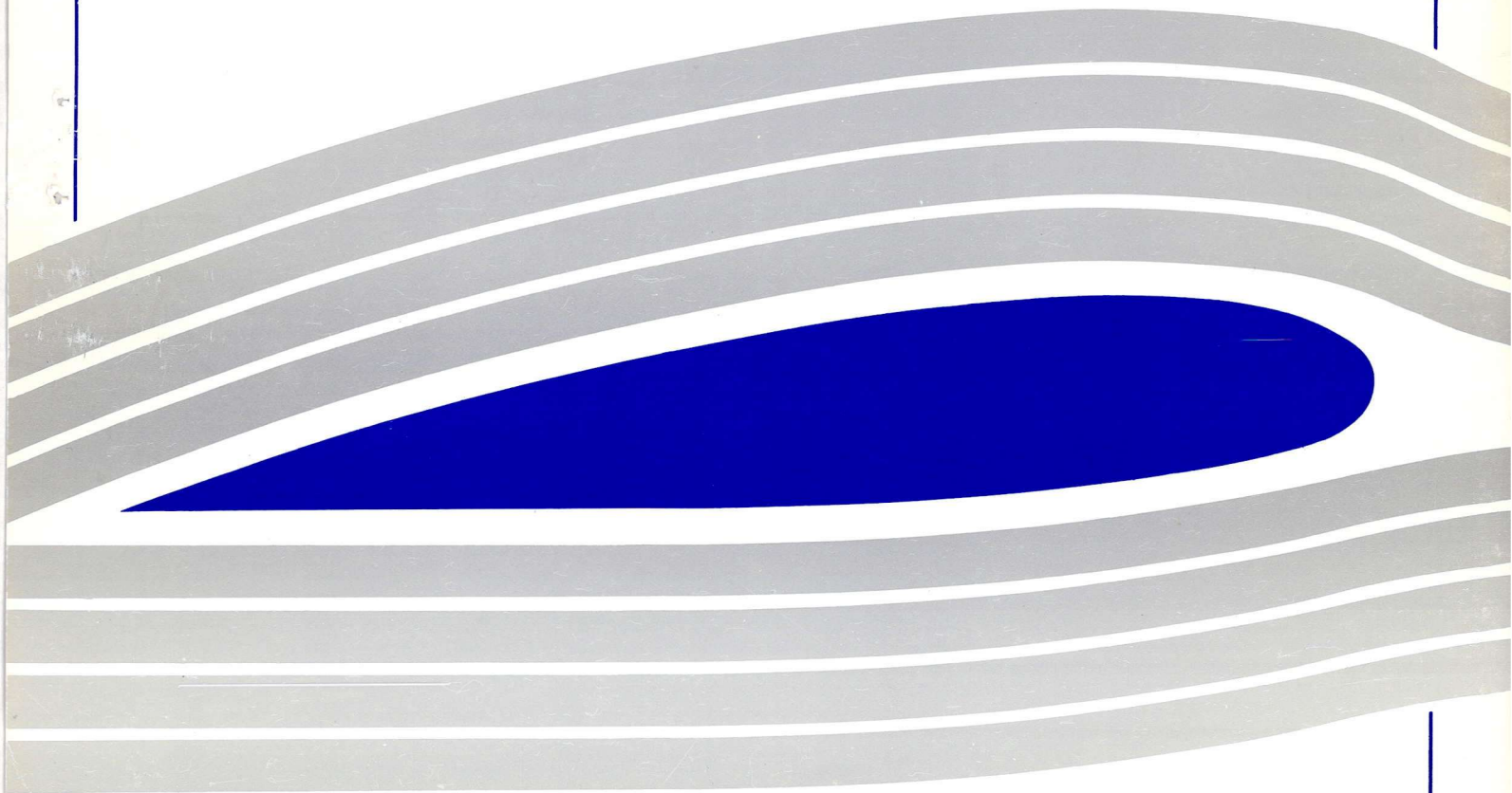

Multidomain Solutions of Incompressible Flows with Complex Geometry by Generalized Differential Quadrature

Chang SHU and Bryan E. RICHARDS

G.U. Aero. Report 9118

November, 1991

LIST OF NOTATIONS

t	time
x_i	coordinates in the horizontal direction
y_i	coordinates in the longitudinal direction
N	number of grid points in the x direction
M	number of grid points in the y direction
$f_x^{(n)}(x_i, y_j)$	the *n*th order derivative of function f(x,y) with respect to x at x_i, y_j
$f_y^{(m)}(x_i, y_j)$	the *m*th order derivative of function f(x,y) with respect to y at x_i, y_j
$w_{ik}^{(n)}$	weighting coefficients for the discretization of $f_x^{(n)}(x_i, y_j)$
$\overline{w}_{jk}^{(m)}$	weighting coefficients for the discretization of $f_y^{(m)}(x_i, y_j)$
Ω	whole domain
Ω_i	the *i*th subdomain
Ω_j	the *j*th subdomain
Γ	the physical boundary of a problem
Γ_{ij}	the interface between Ω_i and Ω_j
x_k^i, y_k^i	local coordinates in the *i*th subdomain
x_k^j, y_k^j	local coordinates in the *j*th subdomain
a_{mn}^i	weighting coefficients of the first order derivative in the *i*th subdomain
a_{mn}^j	weighting coefficients of the first order derivative in the *j*th subdomain
$\underline{f}$	the functional value at the interface
f_z	the first order derivative of function f with respect to z
u	horizontal velocity component
v	vertical velocity component
ω	vorticity
ψ	stream function
Re	Reynolds number
ν	kinetic viscosity

ω_{ij}, ψ_{ij}, u_{ij}, v_{ij}	values of ω, ψ, u, v at x_i, y_j
U_{max}	maximum value of velocity at the inlet for backward facing step problem
D	inlet width for problem of backward facing step
h	the height of the step for flow past a square step
$\underline{x}_{up}$	length of the upstream separation zone, non-dimensionalized by the height of step for flow past a square step
$\underline{x}_{do}$	length of the downstream separation zone, non-dimensionalized by the height of step for flow past a square step

ABSTRACT

A multi-domain generalized differential quadrature method for the solution of two-dimensional, steady, incompressible Navier-Stokes equations in the stream function-vorticity formulation around an arbitrary geometry is presented, and applied to the flows past a backward facing step and a square step in a channel. In each subdomain, the spatial derivatives are discretized by local generalized differential quadrature. The resultant set of ordinary differential equations for vorticity are solved by the 4-stage Runge-Kutta scheme, and the set of algebraic equations for the stream function are solved by LU decomposition. Patching conditions at the interface of subdomains are used. A residual averaging technique is applied to accelerate the convergence to steady state resolution. Good agreement is obtained, compared with available experimental data and other numerical results even though only a few grid points are used.

1. INTRODUCTION

For simulation of physical problems, low order finite difference and finite element methods are used extensively. Generally, these methods require a large number of grid points for the solution of the relevant partial differential equations in order to achieve reasonable accuracy. More recently, the global techniques of spectral and pseudospectral methods have achieved considerable success in obtaining solutions to engineering problems with moderate accuracy, using only a few grid points. But, since these methods do not discretize the derivatives directly, they may be inconvenient to use, especially for the case with nonlinear terms and high order derivatives. On the other hand, since the coordinates of grid points in spectral methods are usually taken as the roots of a specific function, a transformation between the physical space and the computational space is often required. In seeking a more efficient numerical method, the current authors have developed a method, based on the work of Bellman et al [1], of generalized differential quadrature (GDQ) [2], which is also a global method and is easier to apply than spectral methods. It is shown in Ref. 2 that GDQ can be considered as the highest order finite difference scheme, and both GDQ and the Chebyshev pseudospectral method provide exactly the same weighting coefficients of the first order derivative if the coordinates of grid points are chosen as the roots of a Chebyshev polynomial. This demonstrates that GDQ may have a considerable scope for development since it does not require the base polynomials

to be orthogonal and can be used with arbitrary distributions of grid points. The main features of GDQ is its high order accuracy, global convergence, ease of application and programming. The application of GDQ to the solution of incompressible flows such as the natural convection in a square cavity, driven cavity flow and the flow past a circular cylinder, has been shown to be successful in Refs. 2 and 3. Only a few grid points are needed to give equivalent accurate results compared with low order finite difference and finite element methods using a large number of grid points.

GDQ however has still encountered some difficulty in application. One difficulty is the time step size limitation for an explicit scheme with a large number of grid points. This difficulty can be overcome by use of, for example, implicit schemes and multi-domain techniques. GDQ generally requires the computational domain to be rectangular in the same way as the spectral method, but in practical applications, the physical domains are usually complex, leading to difficulties in numerical simulation. These difficulties can be alleviated by the choice of grid generation and by multi-domain techniques. In addition, the multi-domain technique is suited to the case in which there are geometrical singularities such as corners and sharp edges tackled and discussed in this paper or the case where the computational domain may be divided into several regions described by different differential equations. Example of the latter category includes the viscous region near the surface of a solid body modelled by the Navier-Stokes equations, and the inviscid region far from the solid boundary by the Euler equations.

The present paper is devoted to the presentation and application of a multi-domain generalized differential quadrature technique for solving the incompressible Navier-Stokes equations in stream function-vorticity formulation. This approach combines the geometric capabilities of the multi-domain technique with the potential for high order accuracy of GDQ. The problem studied are the flows past a backward facing step and a square step. These are cases that have been extensively used for validating numerical techniques.

2. THE NUMERICAL TECHNIQUE

2.1 Generalized Differential Quadrature

The global method of differential quadrature (DQ), firstly presented by Bellman et al [1], expresses a partial derivative of a function with respect to a coordinate direction as a weighted linear sum of all the functional values at all mesh points along that direction. The key technique in DQ is to determine the weighting coefficients for any order derivative. Bellman suggested two ways to determine the weighting coefficients of the first order derivative. One solves a set of algebraic equations. Unfortunately, for a large number of grid points, the matrix of this equation system is ill-conditioned, and therefore, its inversion is difficult. The other computes the weighting coefficients by a simple algebraic formulation, but with the coordinates of grid points chosen as the roots of a shifted Legendre polynomial. This means that if the number of grid points is specified, the distributions of grid points are the same for different physical problems. This, however, may provide a major drawback and restrict the application of this technique. In order to overcome the drawbacks for DQ, the technique of generalized differential quadrature (GDQ) was then developed [2]. GDQ determines the weighting coefficients of the first order derivative by a simple algebraic formulation without any restriction on choice of grid points. The weighting coefficients of the second and higher order derivatives are determined by a recurrence relationship. For details, see Ref. 2. Here for brevity, only the results of the two-dimensional case are given. The nth order partial derivative of function f(x,y) with respect to x at x_i and y_j, $f_x^{(n)}(x_i, y_j)$, and the mth order partial derivative of f(x,y) with respect to y at x_i and y_j, $f_y^{(m)}(x_i, y_j)$, are discretized by

$$f_x^{(n)}(x_i, y_j) = \sum_{k=1}^{N} w_{ik}^{(n)} \cdot f(x_k, y_j) \tag{1}$$

$$f_y^{(m)}(x_i, y_j) = \sum_{k=1}^{M} \overline{w}_{jk}^{(m)} \cdot f(x_i, y_k) \tag{2}$$

for i = 1, 2, ···, N; j = 1, 2, ···, M; n = 1, 2, ···, N-1; m = 1, 2, ···, M-1

where x_i: i = 1, 2, ···, N; y_j: j = 1, 2, ···, M, are the coordinates of grid points in the x and y direction, $w_{ij}^{(n)}$, $\overline{w}_{ij}^{(m)}$ are the weighting coefficients, which can be determined as follows

$$w_{ij}^{(1)} = \frac{M^{(1)}(x_i)}{(x_i - x_j)\cdot M^{(1)}(x_j)} \quad , \quad i, j = 1, \cdots, N, \ j \neq i \tag{3}$$

$$\overline{w}_{ij}^{(1)} = \frac{P^{(1)}(y_i)}{(y_i - y_j)\cdot P^{(1)}(y_j)} \quad , \quad i, j = 1, 2, \cdots, M, \ j \neq i \tag{4}$$

where

$$M^{(1)}(x_i) = \prod_{k=1, k\neq i}^{N} (x_i - x_k)$$

$$P^{(1)}(y_i) = \prod_{k=1, k\neq i}^{M} (y_i - y_k)$$

$$w_{ij}^{(n)} = n\cdot\left(w_{ij}^{(1)}\cdot w_{ii}^{(n-1)} - \frac{w_{ij}^{(n-1)}}{x_i - x_j}\right) \quad , \quad j \neq i \tag{5}$$

for i, j =1, 2, ···, N; n = 2, 3, ···, N-1,

$$\overline{w}_{ij}^{(m)} = m\cdot\left(\overline{w}_{ij}^{(1)}\cdot \overline{w}_{ii}^{(m-1)} - \frac{\overline{w}_{ij}^{(m-1)}}{y_i - y_j}\right) \quad , \quad j \neq i \tag{6}$$

for i, j = 1, 2, ···, M; m = 2, 3, ···, M-1,

$$w_{ii}^{(n)} = -\sum_{j=1, j\neq i}^{N} w_{ij}^{(n)} \quad , \ i = 1, 2, \cdots, N; \ n = 1, 2, \cdots, N-1 \tag{7}$$

$$\overline{w}_{ii}^{(m)} = -\sum_{j=1, j\neq i}^{M} \overline{w}_{ij}^{(m)} \quad , \ i = 1, 2, \cdots, M; \ m = 1, 2, \cdots, M-1 \tag{8}$$

Finally, if the functional values at all collocation points are obtained, it is easy to determine the functional values in the overall domain by means of the polynomial approximation, i.e.

$$f(x, y_j) = \sum_{i=1}^{N} f(x_i, y_j)\cdot r_i(x) \tag{9}$$

$$f(x_i, y) = \sum_{j=1}^{M} f(x_i, y_j)\cdot s_j(y) \tag{10}$$

$$f(x, y) = \sum_{i=1}^{N}\sum_{j=1}^{M} f(x_i, y_j)\cdot r_i(x)\cdot s_j(y) \tag{11}$$

where $r_i(x)$, $s_j(y)$ are the Lagrange interpolation polynomials along the x and y direction respectively.

2.2 Multi-Domain Technique

The physical domain of the problem can be represented by Ω, and the boundary by Γ. The multi-domain technique, firstly, decomposes the domain Ω into several subdomains Ω_i, i = 1,

···, K, where K is the number of subdomains. In each subdomain, a local mesh can be generated with stretching near the boundary and a local high order polynomial approximation such as the local GDQ technique can be used, in the same fashion as the application of GDQ in a single domain. In the case of solving the incompressible Navier-Stokes equations, this means that the resultant ordinary differential equations for vorticity and the algebraic equations for stream function are to be solved in each subdomain. Each subdomain may have a different number of grid points. The solutions for interior grid points are independent for each subdomain, thus they can easily be computed in parallel. Globally, the information exchange between subdomains is required. This can be done across the interface of subdomains. Since any complex geometry can be transformed into a rectangular domain or a combination of the rectangular subdomains, by the technique of grid generation. Here we only consider the rectangular domain for demonstration without losing generality. Supposing Γ_{ij} is the interface between the subdomain Ω_i And Ω_j, that is

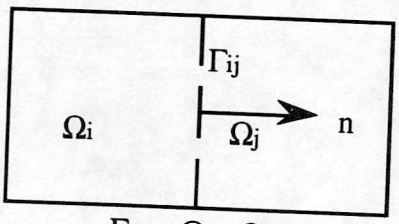

$\Gamma_{ij} = \Omega_i \cap \Omega_j$

The patching condition is enforced at the interface Γ_{ij} so that both the function and its first order derivative normal to Γ_{ij} are continuous along the normal direction of the interface, i.e.

$$f(x_N^i) = f(x_1^j) \quad on \quad \Gamma_{ij} \tag{12}$$

$$f_n(x_N^i) = f_n(x_1^j) \quad on \quad \Gamma_{ij} \tag{13}$$

where $f(x_N{}^i)$, $f(x_1{}^j)$ represent the values of the function f at the interface of the i subdomain and the j subdomain, and $f_n(x_N{}^i)$, $f_n(x_1{}^j)$ the values of the first order derivative of f with respect to n at the interface.

For the cases selected for study, each subdomain is rectangular. Then the normal direction to the interface is parallel to one coordinate axis in the local coordinate system. For simplicity, this coordinate axis can be assumed as the x axis, and along this direction, there are N grid points in the i subdomain and M grid points in the j subdomain. The weighting coefficients of the first order derivative along the x direction are written as $a_{mn}{}^i$ in the i subdomain and $a_{mn}{}^j$ in the j

subdomain. Thus, using the technique of GDQ, equation (13) can be written as

$$\sum_{k=1}^{N} a_{Nk}^{i} \cdot f(x_k^i) = \sum_{k=1}^{M} a_{1k}^{j} \cdot f(x_k^j) \tag{14}$$

Using (12), and setting $f(x_N^i) = f(x_1^j) = \underline{f}$, we obtain

$$\underline{f} = \frac{\sum_{k=1}^{N-1} a_{Nk}^{i} \cdot f(x_k^i) - \sum_{k=2}^{M} a_{1k}^{j} \cdot f(x_k^j)}{a_{11}^{j} - a_{NN}^{i}} \tag{15}$$

where $\underline{f}$ is the value of the function f at the interface Γ_{ij}, which exchanges the information between the subdomains, and the $f(x_k^i)$, $f(x_k^j)$ represent the values of the function f at x_k^i in the i subdomain and x_k^j in the j subdomain. For the solution of the incompressible Navier-Stokes equations in the vorticity-stream function formulation, $\underline{f}$ can be the vorticity and stream function, and equation (15) is used as the Dirichlet boundary condition for them in the subdomain at each time step. Equation (15) is suitable for the rectangular domains. If the computational domain is a non-rectangular domain, it should be transformed into a rectangular domain or a combination of several rectangular subdomains firstly, then equation (15) can be applied.

3. GOVERNING EQUATIONS AND NUMERICAL DISCRETIZATION

The two-dimensional, time-dependent, incompressible Navier-Stokes equations can be written, in the vorticity-stream function dimensionless formulation as

$$\omega_t + u \cdot \omega_x + v \cdot \omega_y = \nabla^2 \omega / \mathrm{Re} \tag{16}$$

$$\nabla^2 \psi = \omega \tag{17}$$

where ω, ψ, Re are the vorticity, stream function and Reynolds number, ∇^2 is the Laplacian operator, and f_z represents the first order derivative of f with respect to z, with f representing ω and ψ and z representing t, x and y, The symbols u, v are the components of the velocity in the x and y direction, which can be calculated from the stream function

$$u = \psi_y$$

$$v = -\psi_x$$

Equations (16), (17) are suitable for full flow fields. We let (16), (17) be satisfied in the interior

grid points of each subdomain. For simplicity, the case of discretization in the subdomain Ω_i, where there are N grid points in the local x direction and M grid points in the local y direction, is chosen for demonstration. When the derivatives are approximated using the method described in the previous section, the discretized forms of (16-17) become

$$\frac{d\,\omega_{ij}}{dt} + u_{ij} \cdot \sum_{k=1}^{N} w_{ik}^{(1)}\, \omega_{kj} + v_{ij} \cdot \sum_{k=1}^{M} \overline{w}_{jk}^{(1)}\, \omega_{ik} = \frac{1}{\mathrm{Re}} \cdot \left[\sum_{k=1}^{N} w_{ik}^{(2)}\, \omega_{kj} + \sum_{k=1}^{M} \overline{w}_{jk}^{(2)}\, \omega_{ik} \right] \tag{18}$$

$$\sum_{k=1}^{N} w_{ik}^{(2)}\, \psi_{kj} + \sum_{k=1}^{M} \overline{w}_{jk}^{(2)}\, \psi_{ik} = \omega_{ij} \tag{19}$$

for i = 1, 2, ···, N; j = 1, 2, ···, M.

For the cases selected for study, there are four types of boundaries, inlet boundary, outlet boundary, solid boundary and interface. Physically, the boundary conditions at the inlet and solid boundaries are usually given by the components of velocity. There are several choices of the boundary condition at the outlet boundary. Amongst them, the natural boundary condition (zero gradient) was commonly used. The boundary condition at interfaces can be obtained from the equation (15). For each subdomain, the boundary conditions for vorticity are given by

$$\omega = u_y - v_x \tag{20}$$

at the inlet or the solid boundary, and

$$\omega_x = 0 \tag{21}$$

at the outlet boundary, and equation (15) at the interface. In equations (20), (21), the derivatives can be discretized by GDQ. So there are four conditions for ω in each subdomain, with which, the set of (N-2)×(M-2) ordinary differential equations (18) were solved by the 4-stage Runge-Kutta Scheme [4] where the residual averaging technique [5] was used in order to accelerate the rate of convergence to the steady state resolution. For the case of vorticity-stream function formulation used, the boundary conditions for two components of velocity at the inlet or the solid boundary should be transformed into two boundary conditions for stream function at each boundary. One boundary condition is a Dirichlet type, the other is a Neumann type. After discretizing the derivative for the Neumann condition by GDQ, the Dirichlet and Neumann type conditions can be combined to give two-layer conditions for ψ at each boundary (for details, see Ref. 2). At the outlet boundary, the boundary condition for ψ is given by

$$\psi_x = 0 \tag{22}$$

which can be discretized by GDQ. Similarly, the boundary condition for ψ at the interface can

be obtained from equation (15). As a result, two-layer boundary conditions are used at the inlet or the solid boundary, and a one-layer boundary condition is used at the outlet boundary or the interface. Since, the topography of the boundary may be different for different subdomains, the number of boundary conditions for ψ may be different for different subdomains. Thus the algebraic equation system (19) to be solved for ψ may have different orders for different subdomains. The matrix of equation system (19) is not a sparse one, and thus it can be solved by an iterative or a direct method. Since GDQ can get accurate numerical results using just a few grid points, the order of equation system (19) is not large, and is much less than that given by a low order finite difference scheme. In our cases a direct method of LU decomposition was used to solve equation system (19). The solution procedure can be outlined as follows

(1) give initial values of u, v, ω;

(2) integrate (18) and obtain the values of ω at interior grid points of all the subdomains at the next time step;

(3) solve (19) and obtain the values of ψ at interior grid points of all the subdomains;

(4) calculate the values of ψ at the boundaries and interfaces for all the subdomains;

(5) calculate the new values of u, v in the full flow field;

(6) calculate the values of ω at the boundaries and interfaces for all the subdomains;

(7) if the convergence criterion is satisfied for all the subdomains, then stop; otherwise turn to step (2).

4. THE FLOW PAST A BACKWARD FACING STEP

The flow past a backward facing step is an excellent test case for validating the solver for incompressible separated flows since this flow forms a recirculation zone located between the separation at the step and the reattachment downstream at a distance which increases with Reynolds number Re. There are many numerical results and experimental data for this case available in the literature [6]-[8]. For numerical simulation, the computational domain is divided into 3 subdomains. The problem definition and the computational domain are shown in Figure 1, where the expansion ratio is 1:1.5. All the lengths have been normalized by the inlet width D, and the velocities by the maximum value of the longitudinal velocity at the inlet, U_{max}, which then define the Reynolds number as

$Re = D \cdot U_{max}/\nu$

For this test case, the inlet is located at a distance 6D upstream of the step, and the outlet is located at 12D downstream of this position. A fully developed (pipe flow) parabolic velocity profile is used as the boundary condition for ψ at the inlet, which gives

$$\psi = 2y^2 - 4y^3/3, \quad \psi_x = 0 \qquad \text{at the inlet} \tag{23}$$

and the natural boundary condition

$$\psi_x = 0, \quad \omega_x = 0 \tag{24}$$

is used as the boundary condition at the outlet. At the wall, the no-slip boundary condition is represented by

$$\psi = \begin{cases} 2/3 & \textit{on the upper wall} \\ 0 & \textit{others} \end{cases} \tag{25}$$

and $\psi_n = 0$, where n indicates the normal to the wall

To verify that the solution is independent of the grid, different mesh sizes have been tested. Numerical experiment shows that this case can be accurately simulated using few grid points. The length of recirculation zone computed by the mesh size of 15×13 for domain I, 23×13 for domain II and 23×11 for domain III is less than four percent different from that computed by the mesh size of 15×17 for domain I, 23×17 for domain II and 23×19 for domain III for all Reynolds numbers. In the following, all the results are based on the former mesh sizes respectively shown in Fig. 2.

The sharp corner of the step is a singularity since at this point the second order derivative of ψ, namely ψ_{yy}, is discontinuous along the vertical line. Thus, since this point is on the boundary, not at the corner, of the computational domain, small spurious deviations in vorticity may be produced near the step. This phenomena has been found in Reference [6] and in our own previous results. This behaviour can be removed by such techniques as the interpolated method, the multi-domain scheme, etc. For the present case, the multi-domain technique was used. Since the sharp corner of the step is exactly at the corner of the subdomain, then in each subdomain, equations (18)-(19) are solved without the treatment of the sharp corner of the step.

Numerical results for Reynolds numbers range from 100 to 1000 were obtained. When Re

$\leqslant$ 700, accurate numerical results were obtained within 2 minutes CPU time on an IBM 3090 for each Reynolds number, and when Re > 700, accurate results were obtained within 3.5 minutes CPU time for each Reynolds number. Figure 3 illustrates the computed streamlines for Reynolds numbers of 200, 400, 600, 800, 1000. In the figure the normalized values of the streamlines (ψ/ψ_{max}) are 1.0, 0.9, 0.8, 0.7, 0.6, 0.5, 0.4, 0.3, 0.2, 0.1, 0.0, -0.1, -0.01, -0.001 and the window for plotting these streamlines in the x direction is from x=-2.0 to x=8.0. Figures 4 and 5 illustrate the vorticity distributions for different Reynolds numbers along the lower and upper walls. The dashed lines included in these figures represent the results of the fully developed parabolic profile which would be obtained if the downstream boundary is located at an infinite distance from the step. From these figures, it is clear that no spurious deviations in the vicinity of the step were found and the flow does not become fully developed at the high Reynolds number cases. Figure 6 shows the horizontal velocity profiles for Reynolds numbers of 100 and 900 at the step. The dashed line in this figure represents the parabolic velocity profile imposed at the inlet. It is seen that the velocity profile for the low Reynolds number case was close to the parabolic profile, except for a systematic but small deviation due to the pressure gradient enforced by the step. However, the velocity profile at the high Reynolds number case tended towards the parabolic profile due to the convective term playing a greater role in the flow field. Thus it is suggested that, for a reasonable accuracy, the inlet should be at a distance in front of the step for low Reynolds numbers, but can be imposed at the step for high Reynolds numbers. Figure 7 shows the velocity profiles at the outlet compared with the fully developed parabolic profile represented again by the dashed line. It is, again, shown that at high Reynolds number the velocity profile at the outlet is not fully developed. This demonstrates that outflow boundary conditions of the Neumann-type may give reasonable solutions for a short distance downstream. Figure 8 shows the length of the recirculation zone for different Reynolds numbers. Also included are the experimental data [7] and numerical results by a finite element method [8]. For the present computational case of expansion ratio of 1:1.5, the present results agree well with the experimental data for low Reynolds numbers, but are under-estimated for high Reynolds numbers.

5. THE FLOW PAST A SQUARE STEP

Now considered is the flow in a channel containing a square step in which the step is located fairly close to the inlet as illustrated in Fig. 9. The flow past a square step with a "flat" inlet velocity distribution rather than a fully developed parabolic profile, is a more challenging problem for numerical simulation since in this case, not only the two sharp corners of the step produce vorticity singularities, but also the boundary condition at the inlet introduces other vorticity singularities. Hughes et al [9] presented several results using the FEM and claimed that the conventional Galerkin method produced spurious wiggles in the velocity vectors upstream of the step. They suggested the use of an upwind method which then generated a solution without wiggles. Leone and Gresho [10] studied this problem exhaustively using a velocity-pressure formulation and the conventional Galerkin method, and claimed that the spurious wiggles of the solution may be caused by a combination of the following factors:

(1) Too coarse a grid to resolve the steep gradient occurring in the direction of flow

(2) Inlet boundary conditions and the resulting leading edge singularities

(3) Proximity of the inlet region to the step

(4) The sharp edge singularity at the leading corner of the step

They firstly studied Stokes flow and found that the inlet wiggles are caused by the leading edge singularities (high pressures are generated at the corners where the fluid decelerates and converges toward mid-channel). They then studied viscous flow using the Navier-Stokes equations and claimed that, when a coarse mesh is used the inlet wiggles may be caused more by the presence of the step than the leading edge singularity, and when the finer mesh is used, most of the inlet wiggles disappear, only small deviations appearing near the top singularity of the inlet leading edge. They thus suggested that this difficult problem should be solved on a fine grid.

Following Hughes et al., it was attempted to simulate the developing flow in a one unit high (the characteristic length for defining Reynolds number Re) channel containing a step located at 1.2 units from the inlet which is 0.4 units high and 0.4 units across. The problem definition and the computational domain are shown in Figure 9, where the overall domain is decomposed into 5 subdomains with 4 interfaces. The inlet boundary condition is a "flat" velocity profile, $u = 1$ and $v = 0$, except that the no-slip condition, $u = 0$ occurs on the top and bottom surfaces, which

gives

$$\psi = y \ , \ \psi_x = 0 \qquad \text{at the inlet} \tag{26}$$

and the boundary condition

$$\psi_x = 0 \ , \ \omega_x = 0 \tag{27}$$

is imposed at the outlet. On the walls and the surface of the step, the no-slip boundary condition gives

$$\psi = \begin{cases} 1 & \textit{on the upper wall} \\ 0 & \textit{others} \end{cases}$$

and $\psi_n = 0$, where n is the normal to the surface.

For the present numerical simulation, the outlet location is chosen as 8 units from the inlet. Numerical experiment showed that the accurate results can be obtained by using the mesh sizes of 15×13 for domain I and II, 7×13 for domain III, 21×13 for domain IV and V. This configuration is shown in Figure 10. Using the same approach as for the backward facing step, the multi-domain solutions of this problem for Reynolds numbers range from 25 to 250 were obtained. For each Reynolds number, the accurate numerical results were obtained within 4 minutes of CPU time on the IBM 3090. Figure 11 shows the streamlines for Reynolds numbers of 50, 100, 150, 200, 250, where the values of these streamlines are 1.0, 0.9, 0.8, 0.7, 0.6, 0.5, 0.4, 0.3, 0.2, 0.1, 0.0, -0.1, -0.01, -0.001 and the window for plotting these streamlines in the x direction is from x=0.0 to x=6.0. Clearly, it is shown that no wiggles appear in the flow field except for very small wiggles caused by the top singularity of the channel leading edge, which appear near the top corner of the inlet (streamlines have a small contraction towards mid-channel). This agrees well with the analysis of Leone et al and demonstrates that the mesh sizes used are fine enough to get accurate results. Figure 12 shows the vorticity distributions along the lower wall before the step for different Reynolds numbers. The plots display clearly a large influence of the lower singularity of the channel leading edge on the flow near the inlet. In the region close to the bottom corner of the inlet, the flow is dominated by the high pressure gradient produced mainly by the singularity rather than by viscosity, since in this region, the vorticity is independent of the Reynolds number. Figure 13 shows the vorticity distributions along the lower wall behind the step for different Reynolds numbers. The dashed line included in this figure is the result of the fully developed parabolic profile which would be obtained if the outlet is placed at an infinite distance from the inlet. One can see from Fig. 13 that most cases

except for Re = 50 do not achieve a fully developed parabolic velocity profile at the outlet. This demonstrates that the Neumann-type boundary condition imposed at the outlet can provide reasonable solutions when the outlet is placed only a short distance downstream. Figure 14 shows the vorticity distributions along the surface of the step. The two singularities at the sharp corners are shown clearly. Figure 15 displays the vorticity distributions along the upper wall for different Reynolds numbers. It shows that the flow near the upper singularity of the inlet is dominated by the high pressure gradient, produced mainly by the singularity since the vorticity in this region is shown to be independent of the Reynolds number. This demonstrates that the small deviations in streamlines occurring near the upper corner of the inlet is indeed caused by the singularities at the inlet leading edge. There are some wiggles in (1.2, 1.6) for Re $\geqslant$ 100, which are caused by the singularities of the two sharp corners of the step. The dashed line included in Fig. 15 is again the result of the fully developed parabolic profile. Figure 16 displays the velocity profiles at the outlet for Reynolds number cases of 50 and 250. The plots show that the velocity for the low Reynolds number case achieves a nearly parabolic profile at the outlet. This is not the case for the high Reynolds number case. The lengths of the upstream and downstream separated zone for the various Reynolds numbers are shown in Table I, where $\underline{x}_{up} = x_{up}/h$, $\underline{x}_{do} = x_{do}/h$, x_{up} and x_{do} represent the lengths of the upstream and downstream separation zones, and h is the height of the step.

Table I The Lengths of Upstream and Downstream Eddy

Re	25	50	85	100	150	200	250
$\underline{x}_{up}$	0.1749	0.1749	0.1749	0.1757	0.1777	0.5771	0.5846
$\underline{x}_{do}$	1.5771	2.6701	3.8876	4.3501	5.7549	7.0636	7.9824

6. CONCLUSIONS

The multi-domain generalized differential quadrature (GDQ) technique for the solution of the incompressible Navier-Stokes equations is presented, which combines the geometric capabilities of the multi-domain technique with the potential for high order accuracy of GDQ. Within the problems studied, 3 subdomains were used for the flow in a channel with a backward facing

step and 5 subdomains for the equivalent configuration but with a square step. At the interface of the subdomains, patching conditions were used to enforce both the function of vorticity and stream function as well as their normal derivatives to be continuous across the interface. The natural boundary condition (i.e zero gradient) was used at the downstream boundary for both test cases, and this is shown to be reasonably valid and efficient. Numerical experiment showed that the multi-domain GDQ technique can achieve accurate results by using just a few grid points.

REFERENCES

1. R. Bellman, B.G. Kashef and J. Casti, 'Differential Quadrature: A Technique for the Rapid Solution of Nonlinear Partial Differential Equations', *J. Comput. Phys.* **10**, (1972), 40-52
2. C. Shu, 'Generalized Differential-Integral Quadrature and Application to the Simulation of Incompressible Viscous Flows Including Parallel Computation', *PhD Thesis*, University of Glasgow, July 1991
3. C. Shu and B.E. Richards, 'High Resolution of Natural Convection in a Square Cavity by Generalized Differential quadrature', *in Proceedings of 3rd Int. Conf. on Advances in Numerical Methods in Engineering: Theory and Applications*, Swansea, U. K., Jan. 1990, (eds by Pande and Middleton), Volume **II**, 978-985
4. J. Pike and P.L. Roe, 'Accelerated Convergence of Jameson's Finite Volume Euler Scheme Using Van Der Houwen Integrators', *Comput. Fluids* **13**, 223 (1985)
5. N. Satofuka, K. Morinishi and H. Tokunaga, 'Numerical Solution of the Euler Equations Using Rational Runge-Kutta Method', *Notes on Numerical Fluid Mechanics* **13**, Vieweg, Braunschweig, (1986)
6. A. Ecer, R.K. Rout and P. Ward, 'Laminar Flow past a Backward Step', *Notes on Numerical Fluid Mechanics*, Vol. **9**, Vieweg, Braunschweig, (1984)
7. J.L. Kueny and G. Binder, 'Viscous Flow over Backward Facing Steps: An Experimental Investigation', *Notes on Numerical Fluid Mechanics*, Vol.**9**, Vieweg, Braunschweig, (1984)
8. M. Bredif, 'Calculation of Laminar Flow over a Step by a Finite Element Method Based on the Stream Function-Vorticity Formulation', *Notes on Numerical Fluid Mechanics*, Vol. **9**, Vieweg, Braunschweig, (1984)
9. T.J.R. Hughes, W.K. Liu and A. Brooks, 'Finite Element Analysis of Incompressible Viscous Flows by the Penalty Function Formulation', *J. Comput. phys.* **30**, 1 (1979)
10. J.M., Leone, Jr. and P.M. Gresho, 'Finite Element Simulations of steady, Two-Dimensional, Viscous Incompressible Flow over a Step", *J. Comput. Phys.* **41**, 167-191, (1981)

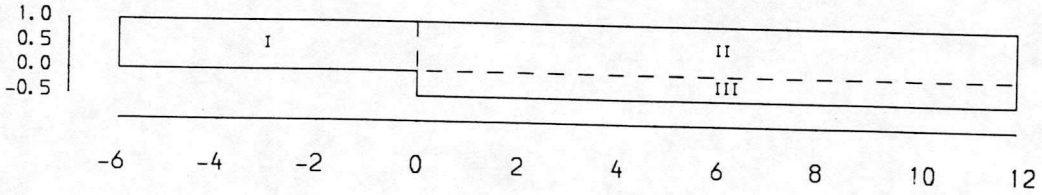

Fig. 1 Problem Definition and Computational Domain for Flow past A Backward Facing Step

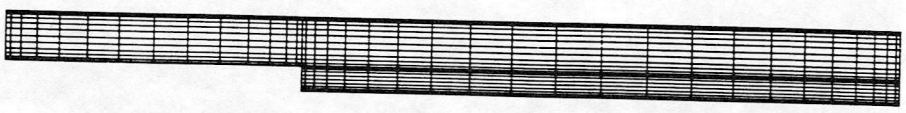

Fig. 2 Meshes for Flow past A Backward Facing Step

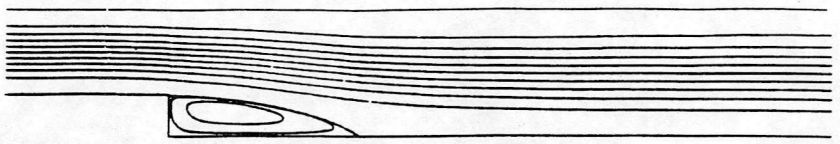

(a) Re = 200

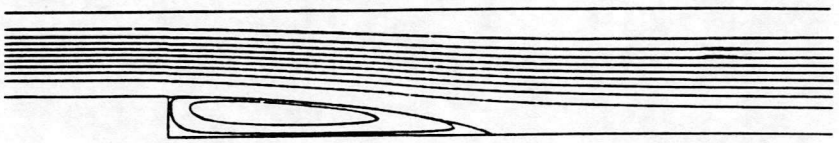

(b) Re = 400

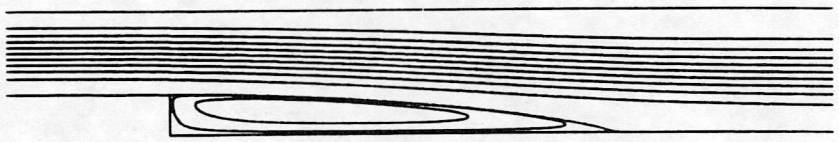

(c) Re = 600

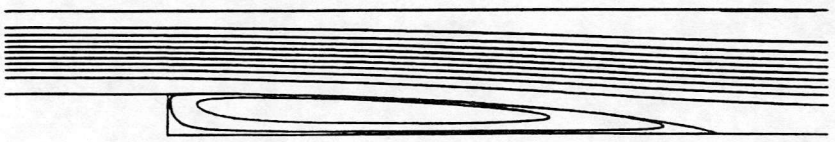

(d) Re = 800

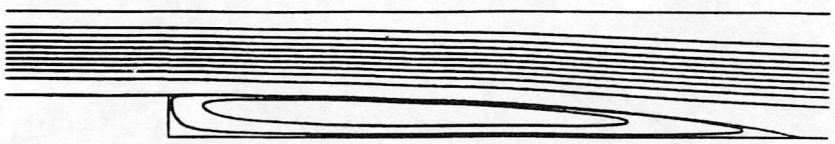

(e) Re = 1000

Fig. 3 Streamlines of the Flow past A Backward Facing Step

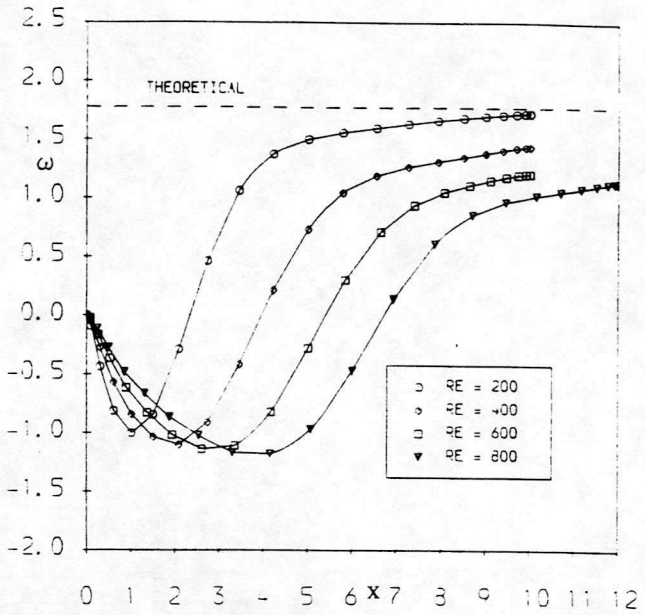

Fig. 4 Vorticity along the Lower Wall for Flow past A Backward Facing Step

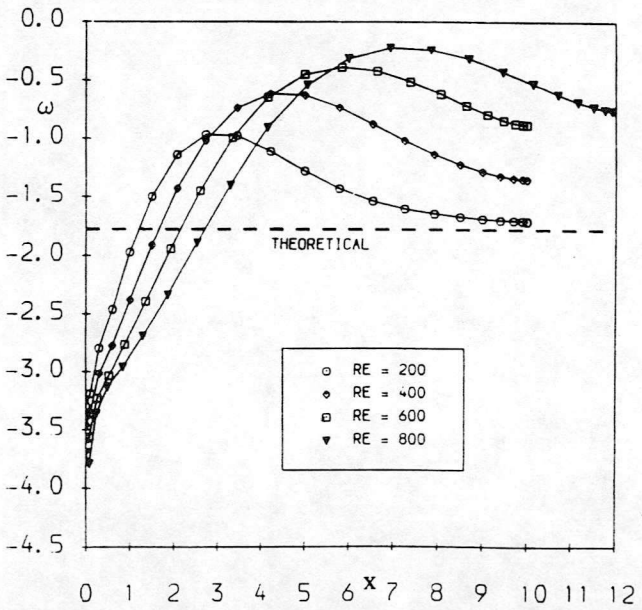

Fig. 5 Vorticity along the Upper Wall for Flow past A Backward Facing Step

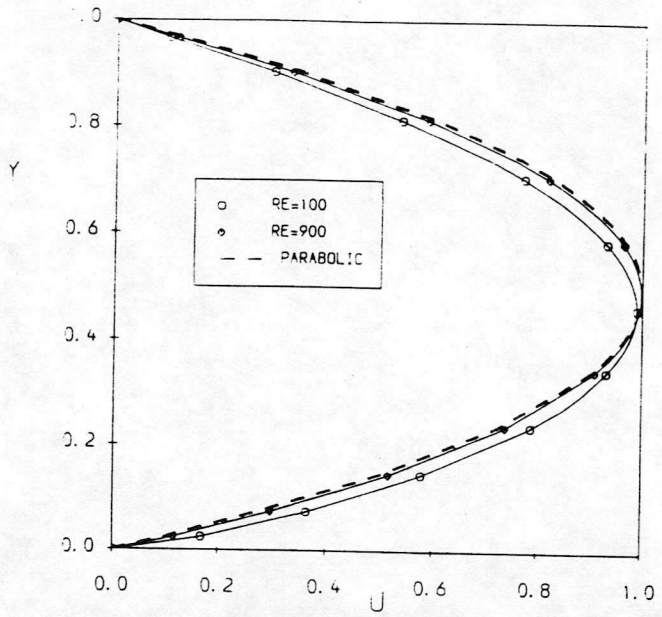

Fig. 6 Horizontal Velocity Profiles at the Backward Facing Step

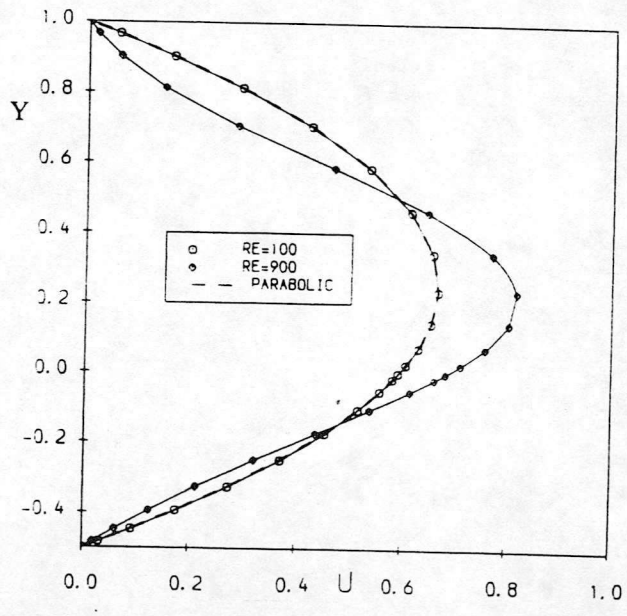

Fig. 7 Horizontal Velocity Profiles at the Outlet of A Backward Facing Step

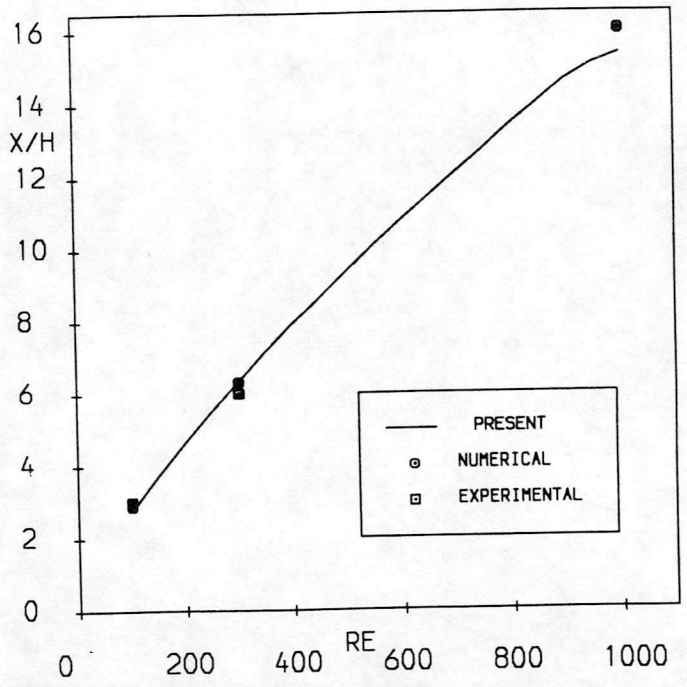

Fig. 8 Length of Recirculation Zone vs Reynolds Number

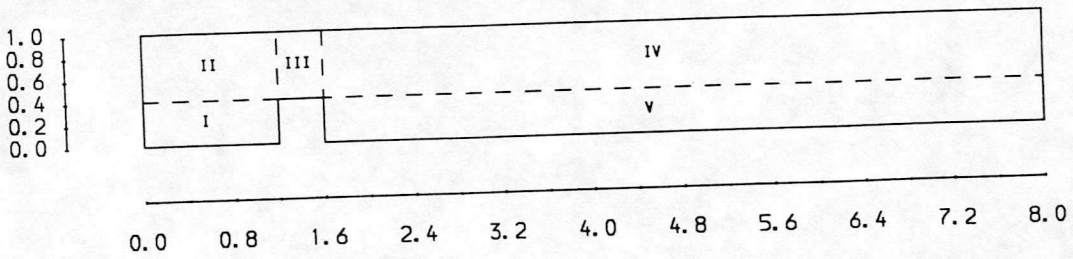

Fig. 9 Problem Definition and Computational Domain for Flow past A Square Step

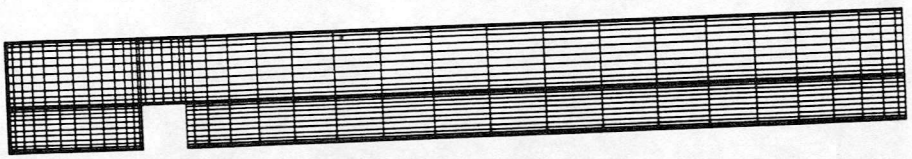

Fig. 10 Meshes for Flow past A Square Step

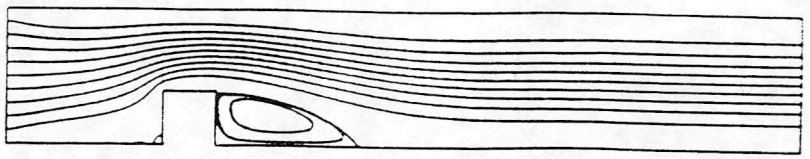

(a) Re = 50

(b) Re = 100

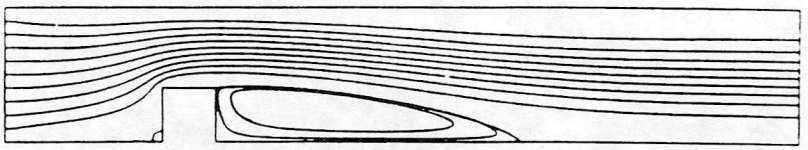

(c) Re = 150

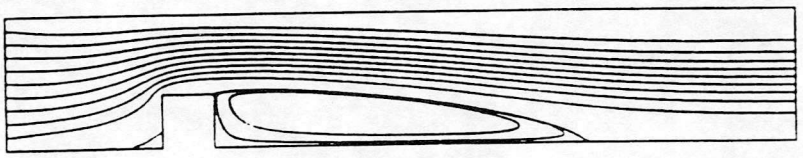

(d) Re = 200

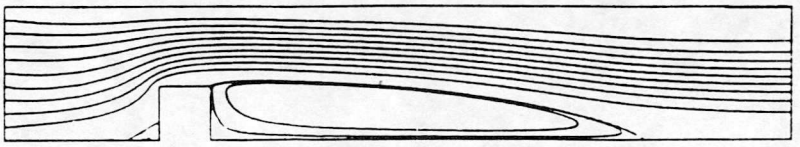

(e) Re = 250

Fig. 11 Streamlines of the Flow past A Square Step

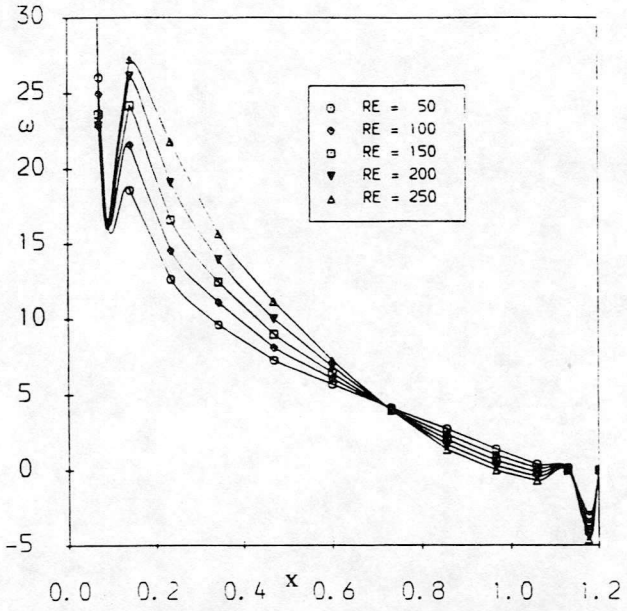

Fig. 12 Vorticity along the Lower Wall before the Square Step

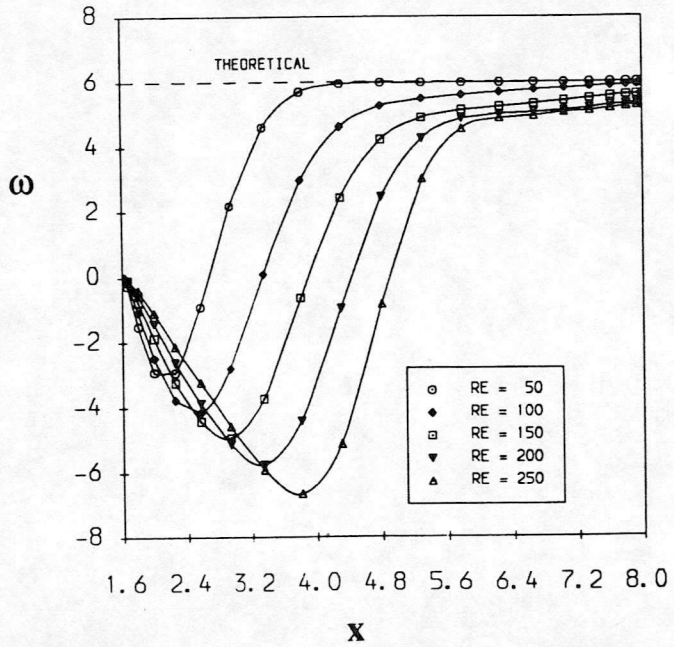

Fig. 13 Vorticity along the Lower Wall behind the Square Step

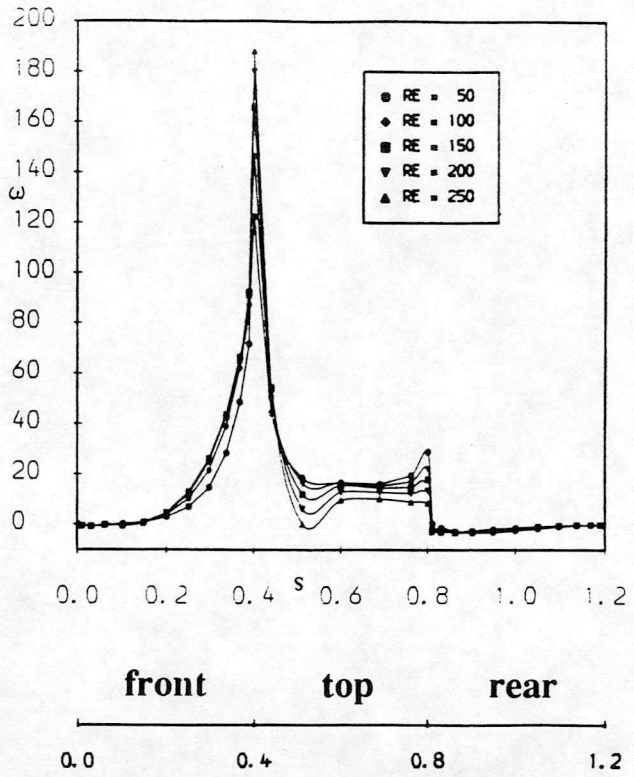

Fig. 14 Vorticity along the Surface of the Square Step

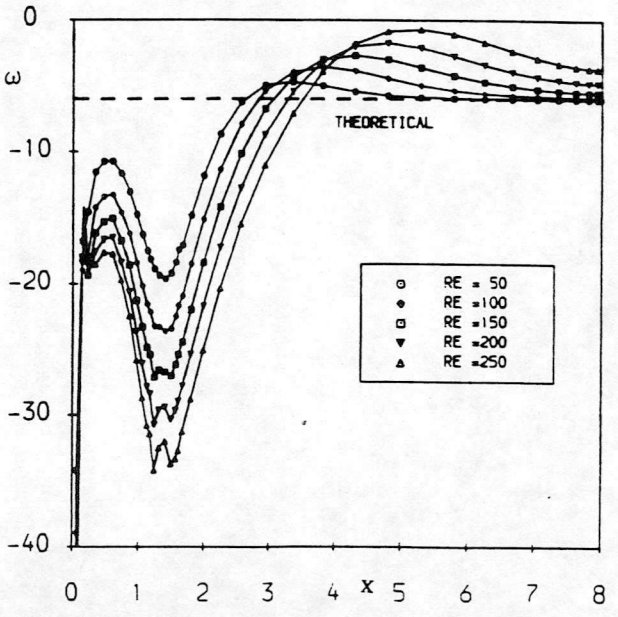

Fig. 15 Vorticity along the Upper Wall for Flow past A Square Step

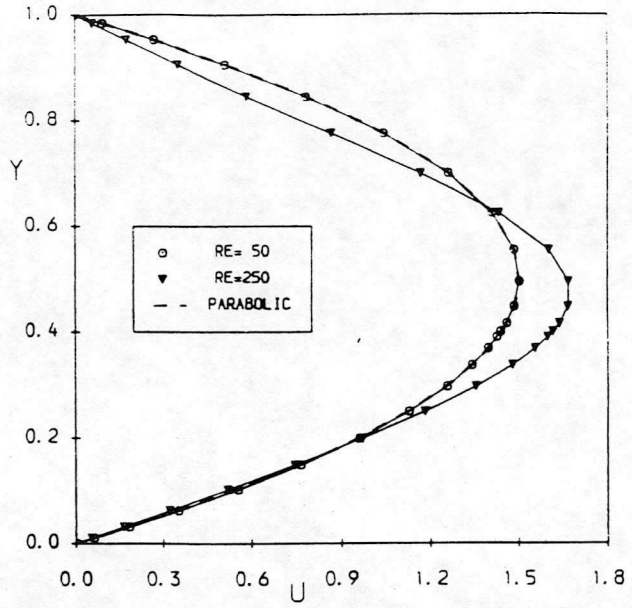

Fig. 16 Horizontal Velocity Profiles at the Outlet of A Square Step